A Micromachined Thermal Wind Sensor

Zhenxiang Yi, Ming Qin, and Qing-An Huang

Contents

Z. Yi (✉) · M. Qin
Key Laboratory of MEMS of the Ministry of Education, Southeast University, Nanjing, China
e-mail: xp@seu.edu.cn; mqin@seu.edu.cn

Q.-A. Huang
Key Laboratory of MEMS of the Ministry of Education, Southeast University, Nanjing, Jiangsu, China
e-mail: hqa@seu.edu.cn

Q.-A. Huang (ed.), *Micro Electro Mechanical Systems*, Micro/Nano Technologies,
https://doi.org/10.1007/978-981-10-5945-2_18

Abstract

This chapter introduces the micromachined thermal wind sensor by MEMS technology. First, three working principles and operation modes are addressed. Then, several typical wind sensors including 1D and 2D devices are presented and the experimental results are given. In order to improve the sensitivity and reduce the power consumption, several methods, such as thinned substrate and low-thermal-conductivity substrate, are presented. Experiments demonstrate that the power consumption has been reduced to less than 20 mW by glass reflow technology. In practice, the MEMS wind sensor can be packaged using DCA package, FC package, and Au-Au bonding package. Despite this, the wind sensor is easy to be affected by the surrounding temperature. Related model is established and verified by the experiments.

Keywords

Wind sensor · Micromachined · MEMS · Thermal conductivity · Full-bridge technology · Package · Environment effect · Temperature difference · Sensitivity · Power consumption

Introduction

Wind sensors are playing an important role in various fields such as agriculture, weather forecast, and transportation. Before, the wind information was obtained by the wind cups and indicators. After that, the ultrasound anemometers were used to realize wind speed measurement based on Doppler effect (Kato et al. 1992). However, these devices cannot meet the requirements of Internet of Things due to big size and high price. Fortunately, the rise of micro-electro-mechanical systems (MEMS) technology pushed the development of the wind sensor and made the devices with small size and low cost possible. There are two kinds of MEMS wind sensors: thermal wind sensors and nonthermal wind sensors. Because of small size and low cost, the thermal wind sensors have been widely researched around the world for a long time. This chapter reviews the progress of the thermal wind sensors and is arranged as following. In section "Principle," the principle of the micromachined thermal wind sensor is introduced. Then, different operation modes are categorized in section "Operation Mode." In section "MEMS Thermal

Wind Sensors," a variety of wind sensors including 1D and 2D sensors are presented. Following, several methods are proposed in order to improve the sensitivity and reduce power consumption in section "Sensitivity Improvement and Power Consumption Reduction." The wind sensors are packaged in section "Package" by different ways. In addition, the environmental effect on the wind sensors is also investigated in section "Environmental Effect." Finally, the conclusion is drawn in section "Conclusion."

Principle

The MEMS thermal wind sensor is based on the effect of wind on the thermal phenomenon. There are three different sensing principles of MEMS thermal wind sensor: hot-wire principle, calorimetric principle, and time-of-flight principle (Kuo et al. 2012).

Hot-Wire Principle

Figure 1 shows the schematic of the wind sensor based on hot-wire principle. An electrical signal is applied on the thermistor and it is heated based on Joul effect. When the wind blows, the heat is taken away. Therefore, the temperature of the thermistor deceases and the wind speed can be resolved by the resistance measurement of the thermistor (Oudheusden 1988; Giani et al. 2002).

The relationship between the heat taken away and the wind speed can be expressed by King's law (1914).

$$P = \left(A + BU^{0.5}\right)\Delta T \tag{1}$$

where P is the heat taken away by the wind, U is the wind speed, ΔT is the temperature difference between the chip and the environment, A and B are determined by the size of the sensor and fluid property. Clearly, the higher the wind speed is, the more the power is taken away. The hot-wire sensor can only measure wind speed while wind direction cannot be obtained.

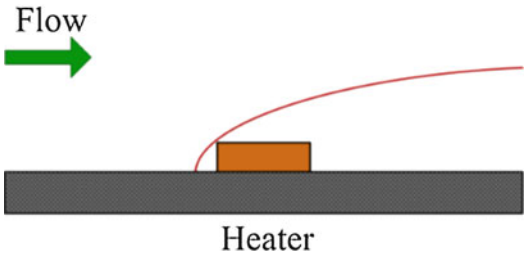

Fig. 1 Schematic of the wind sensor based on hot-wire principle

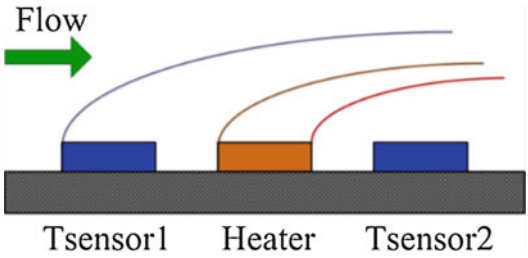

Fig. 2 Schematic of the wind sensor based on calorimetric principle

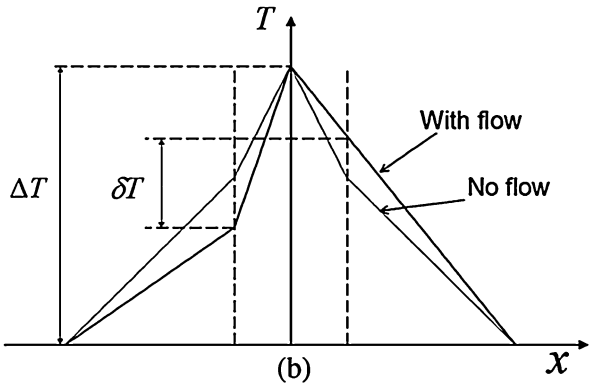

Fig. 3 Temperature distribution of the sensor by calorimetric principle

Calorimetric Principle

As shown in Fig. 2, when an electrical signal is applied, the resistor is heated and the temperature field is formed. Two temperature sensors are placed upstream and downstream with the same distance to the heater. In case of no wind, the temperature field is symmetrical and the temperature T_1 and T_2 is equal. If the wind blows, the temperature field is destroyed and the heat is taken from upstream to downstream. As a result, the temperature upstream decreases while the temperature downstream increases, as shown in Fig. 3. Hence, the wind speed can be deduced by the temperature difference measurement of T_1 and T_2 (Makinwa 2004; Huijsing et al. 1984). The temperature sensor is usually used by thermistor, thermopile, diode, and transistor (Zhu et al. 2014).

In one-dimension (1D) wind sensor, the temperature difference δT between T_1 and T_2 is given by Oudheusden (1990):

$$\frac{\delta T}{\Delta T} = c_0 \frac{k_f W}{k_c D} \left(\frac{L^2}{\nu \rho_c \alpha} \right)^{\frac{1}{3}} \sqrt{U} \tag{2}$$

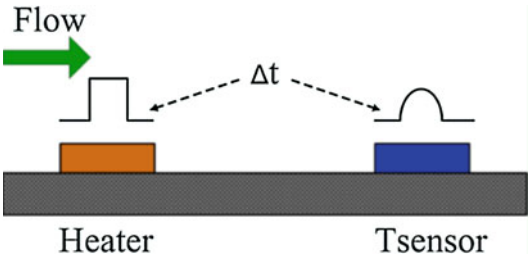

Fig. 4 Schematic of the wind sensor based on time-of-flight principle

where ΔT is the overheated temperature with respect to ambient temperature, W is the chip size of the sensor, k_c and D are the thermal conductivity and thickness of the substrate, respectively. U, k_f, v, and α are the wind speed, the heat conductivity, the kinematic viscosity, and the thermal diffusivity of the flow, respectively. ρ_c is the density of the sensor material. c_0 is the constant which equals 0.08076 when the sensing parts are located on the opposite edges of the sensor.

Time-of-Flight (TOF) Principle

As shown in Fig. 4, for the time-of-fight principle, an electrical pulse is applied to the heater and a thermal pulse is produced. The thermal pulse is taken away by the wind and is detected by the temperature sensor located downstream. Thus, the wind speed can be calculated and given by Wu and Sansen (2002)

$$U = \frac{L}{\Delta t} \tag{3}$$

Where L is the distance between the heater and the temperature sensor, and Δt is the traveling time of the thermal pluse.

In fact, when arriving at the temperature sensor, the thermal pulse is widen in bandwidth and reduced in amplitude due to thermal diffusion. In order to solve this problem, a novel wind sensor by TOF principle is reported (Durst et al. 2003). A continuous periodic current is applied to the heater and the wind speed is extracted by the time lag measurement between the transmitted and received signal.

Operation Mode

For MEMS thermal wind sensors, five operation modes are possible: constant power (CP) mode, constant temperature difference (CTD) mode, temperature balance (TB) mode, constant voltage (CV) mode, and constant current (CC) mode.

Constant Power Mode

In CP mode, the power dissipated in the heater is always kept as a constant. For the hot-wire principle, the heat is taken away by the wind and the temperature of the heater decreases. Finally, the wind speed can be detected by the resistance measurement of the heater. For the calorimetric principle, the sensitivity is high at low speed. However, when the speed increases, the output tends saturation and the measurement range is limited. The reason is that the temperature upstream is no less than that in environment while the temperature downstream is no more than that of the heater. Hence, the temperature difference between upstream and downstream is easy saturation.

Constant Temperature Difference Mode

In order to enhance the dynamic range of the measurement, the CTD mode is presented for thermal wind sensor. In this mode, the power applied to the heater is controlled by the feedback circuits, which make the temperature difference between the heater and the surrounding as a constant. For the hot-wire principle, the heat taken away increases with the wind speed, which decreases the temperature of the heater. In order to realize CTD mode, the heating power is increased, which can represent the wind speed. For the sensor based on calorimetric principle, the saturation speed is increased and the measurement range is enhanced compared with the CP mode.

Temperature Balance Mode

In the TB mode, different parts are heated separately and their temperature is kept balance. Consequently, the information of the wind speed and direction can be extracted by the heated power of all parts. In application, the simplest approach is to divide the chip into four symmetrical parts and heat them to a same temperature. Then, the wind information including speed and direction can be obtained by the four different heating power.

Constant Voltage Mode

Obviously, the CV mode means the applied voltage to the heater is a constant. Sometimes, this mode replaces the CP mode to realize wind speed measurement.

Constant Current Mode

The constant current mode, which make the current through the heater constant, is similar to the CV mode and can also be a substitution for CP mode.

MEMS Thermal Wind Sensors

MEMS thermal wind sensors are categorized into one-dimension (1D) wind sensors and two-dimension (2D) wind sensors. The 1D wind sensors can only measure bidirectional wind speed, while the 2D can realize speed and direction measurement at the same time.

1D Wind Sensors

Gao proposed a 1D wind sensor based on calorimetric principle in Fig. 5 (Gao et al. 2004). The polysilicon line is fabricated as the heater. Polysilicon and Al are connected in series as the thermopile to measure temperature difference based on Seebeck effect. In case of no wind, the temperature distribution is symmetrical and the output voltage upstream equals to that downstream. When the wind blows, the output voltage of the thermopile downstream increases and the voltage of the thermopile upstream decreases. Thus, the wind speed can be resolved by two voltage difference measurement. Different from the hot-wire wind sensor, this design can realize bidirectional measurement. Moreover, anisotropic etching is performed on the front surface of the wafer to reduce thermal loss. The experiment shows that the measurement range is about 0–10 m/s in CTD mode, as shown in Fig. 6.

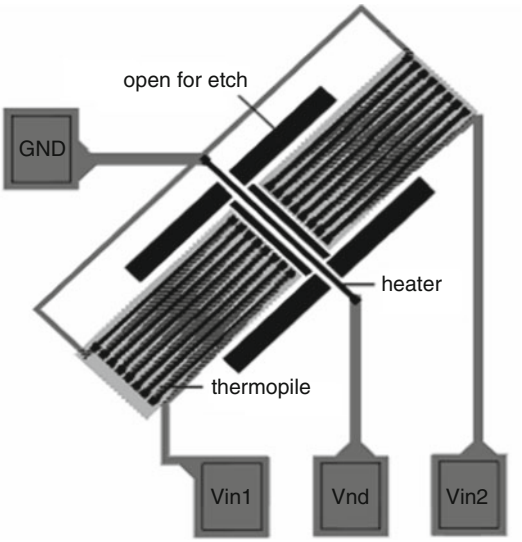

Fig. 5 SEM photograph of the 1D wind sensor

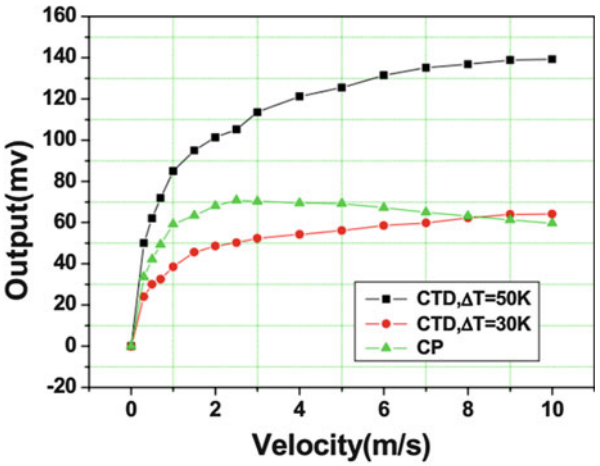

Fig. 6 SEM photograph of the 1D wind sensor

2D Wind Sensors

The 2D wind sensors are categorized into three types depending on different physical transduction methods. First, thermoelectric wind sensor uses thermopile to measure temperature profile based on Seebeck effect. Second, thermoresistive wind sensor makes use of thermistors to detect thermal change. In addition, diodes and transistors are applied to measure temperature in thermoelectronic wind sensor. Trigonometric function method and Gauss fitting method are the two most common ways to realize wind direction measurement.

Thermoelectric Wind Sensor

In 2003, Zhang presented a 2D MEMS wind sensor fabricated by CMOS process (Zhang et al. 2002), as shown in Fig. 7. The heater made of N^+ polysilicon is placed in the center of the sensor chip. Four thermopiles made up of P^+ polysilicon and Al are located in a square around the heater for temperature detection. Both the heater and the thermopiles are fabricated in the silicon dioxide on the surface of the silicon substrate. In order to reduce thermal loss further, the silicon underneath the heater and hot junctions of the thermopiles is removed by front surface etching technology. The operational amplifier circuits are also integrated and the chip area is about 2×1.6 mm. As shown in Fig. 8a, the experiment demonstrates that the output voltage is saturated at the speed of 33 m/s in CP mode. A good sine relationship between the voltage and the direction can be obtained in Fig. 8b. The response time is close to 16 ms when the blowing direction changes.

In 2004, Cheng et al. proposed a 2D wind sensor by CMOS technology based on the work of Zhang in Fig. 9 (Cheng et al. 2004). Instead of front surface etching, back etching technology is applied to reduce thermal loss. Moreover, Al strip is fabricated on the silicon dioxide over the heater in order to increase the temperature of the hot junction of the thermopile. By these two methods, the sensitivity can be

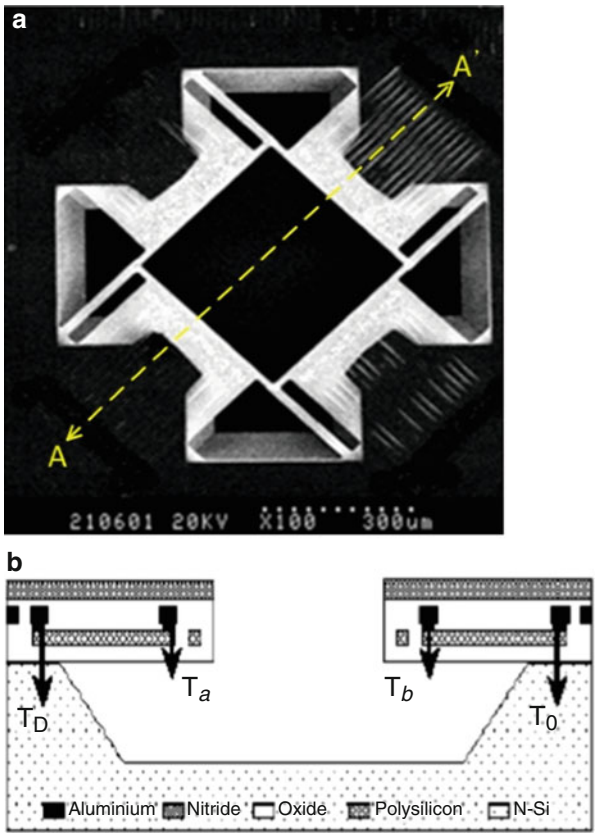

Fig. 7 (**a**) SEM photograph of the wind sensor by Zhang et al. and (**b**) Schematic of the cross-section of AA′

improved. Experiments in Fig. 10 show that this sensor can realize wind speed measurement from 0 to 23 m/s and wind direction measurement of 0–360°.

In 2009, Dong et al. proposed a 2D MEMS wind sensor by standard CMOS MEMS process (Dong 2012). In Fig. 11, polysilicon is fabricated as heater and the thermopiles formed by Al and P^+ polysilicon are used to measure temperature profile resulted by wind. In order to realize CTD mode, a PNP transistor is designed in the center to detect the chip temperature. In Fig. 12a, the wind sensor is tested and the maximum speed is measured to be 40 m/s with the relative error less than 3%. As shown in Fig. 12b, the direction spans from 0° to 360° and the absolute error is less than 3°.

Thermoresistive Wind Sensors

Figure 13a shows the thermoresisitive wind sensor fabricated on silicon substrate (Ye et al. 2017). Ni is used to fabricate heater and thermistors because of high temperature coefficient of resistance (TCR). Al is applied for contacting pads fabrication. In case of no wind, the temperature field is symmetrical and the resistance R1, R2, R3, and R4 is same. When the temperature field is changed by the wind, a resistance of R1 and R3 increases while the other decreases. A Wheatstone bridge including R1 and

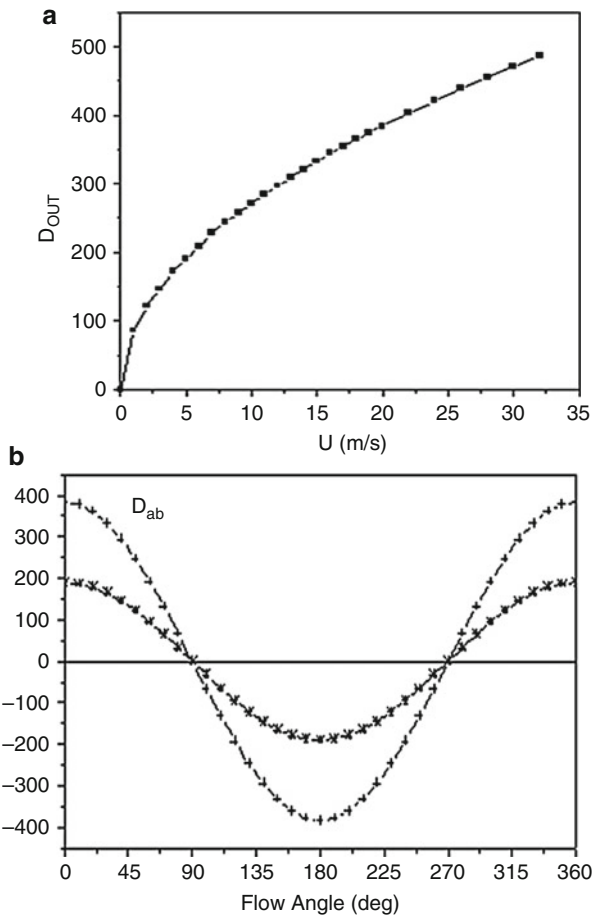

Fig. 8 Experiments of the wind sensor by Zhang et al.: (**a**) wind speed and (**b**) wind direction

R3 is used and the resistance change can be expressed by the output voltage V1, as shown in Fig. 13b. Therefore, the wind speed in north-south direction is obtained. Similarly, the resistance change between R2 and R4 can be extracted by V2, which shows the wind speed in east-west direction. Hence, the total wind speed is resolved by $V_1^2 + V_2^2$ and the wind direction can be deduced by $\tan^{-1}(V^1/V^2)$ based on trigonometric function method. As shown in Fig. 14, this thermoresistive wind sensor exhibits a speed range of 0–30 m/s and direction range of 0–360° in CP mode.

In addition, Shen et al. also presented a thermoresistive wind sensor with different structures on ceramic substrate (Shen et al. 2007). As shown in Fig. 15, one is a traditional square sensor and the other is a circular structure. Pt is fabricated as heater and thermistors on ceramic substrate due to ease of fabrication. The proposed sensor can measure the wind speed from 0 to 10 m/s with the precision of 0.5 m/s. Due to use of ceramic substrate, the power consumption is reduced to less than 50 mW. It should be noticed that the resistance deviation between thermistors cannot be ignored due to poor flatness of ceramic substrate.

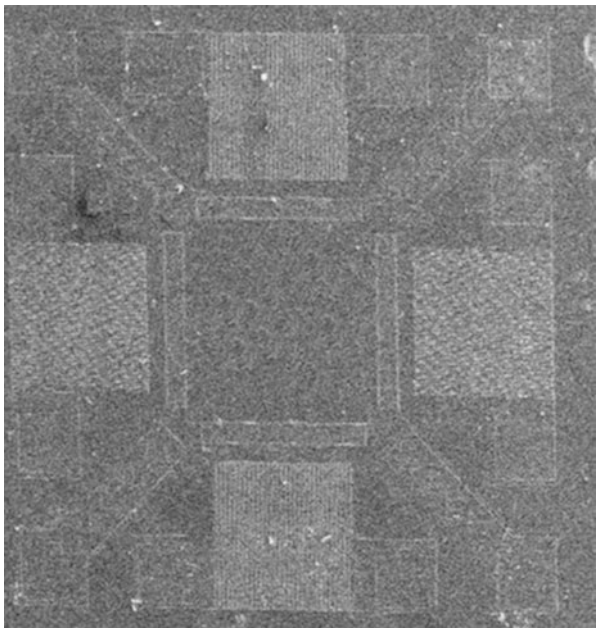

Fig. 9 SEM photograph of the wind sensor by CMOS process

Thermoelectronic Wind Sensors

For diodes and transistors with a fixed current, the breakover voltage decreases with the temperature linearly. This phenomenon can be used to realize temperature detection, and the diodes and transistors are often applied in thermoelectronic wind sensors. In 2001, Qin et al. reported an octagon-structure wind sensor by CMOS process (Qin et al. 2001), as shown in Fig. 16. A ring made of polysilicon is fabricated as heater. Eight laterally polysilicon diodes (LPD) as four pairs are located around the heater symmetrically. The temperature difference between two LDPs in a pair relies on the wind speed. The experiment shows that the temperature coefficient of LPD is about −1.8 mV/K. The presented sensor can realize measurement range of 0 m/s to about 9.5 m/s from eight different directions, as shown in Fig. 17.

In 2006, Wu et al. improved the design of Qin in Fig. 18 (Wu and Qin 2006). The resistors made of Al serve as the heater and temperature sensor of the chip. Hot-wire principle is applied in CTD mode to measure the wind speed. Moreover, eight resistors made of polysilicon are fabricated around the heater for wind direction measurement. In addition, operational amplifiers and three to eight decoders are included in the chip by CMOS process.

In 2007, Sun et al. proposed a new wind sensor operating on CTD mode (Sun 2006), as shown in Fig. 19. The ring heater is made of polysilicon, and eight transistors are applied to measure temperature distribution. The novelty is that a transistor is fabricated in the center to measure the chip temperature. Therefore, the CTD mode is easily realized and the measuring range is up to 30 m/s, as shown in Fig. 20. At the same time, the temperature of eight transistors is measured and the

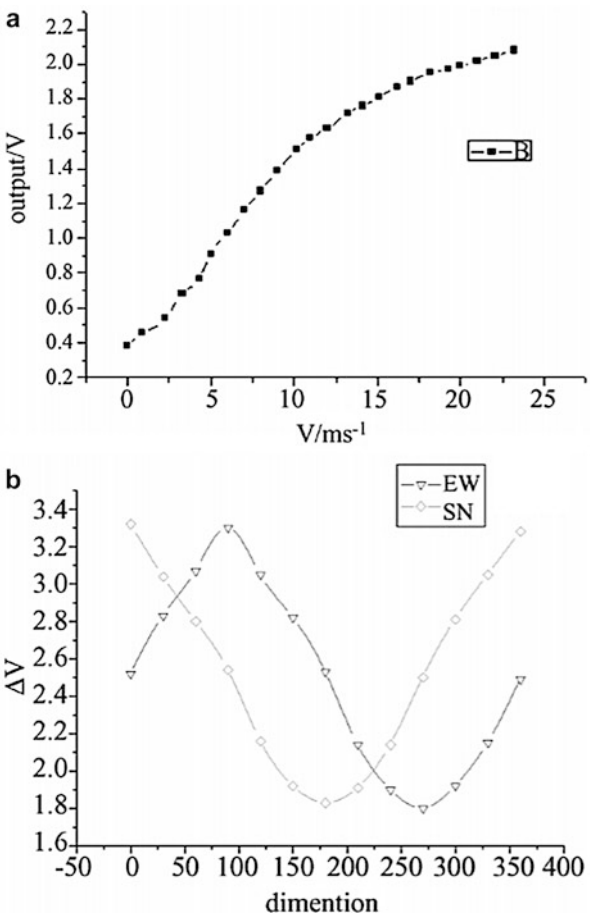

Fig. 10 Measurement of the wind sensor by Cheng: (**a**) wind speed and (**b**) wind direction

wind direction information can be obtained by fitting based on the Gauss function. Figure 21 shows that the wind direction solution is about 10° and the power consumption is no more than 100 mW.

Other Wind Sensors

In 2008, Shen et al. proposed a cross-type wind sensor to realize self-test function (Shen et al. 2008, 2010). As shown in Fig. 22, it is composed of cross-structure heaters and four symmetrically located sensing parts. When the flow angle changes clockwise, the temperature differences among the four parts, namely T_{13} (T_{24}) and T_{12} (T_{14}), will be sine (cosine) functions of the wind direction. Further study shows that the amplitudes of T_{13} and T_{24} are two times of T_{12} and T_{14}, and the phases are 45° before the latter. Then two wind direction values can be obtained for self-test without additional components. As shown in Fig. 23a, the bridge output voltage of the sensor on glass substrate with heating power of 100 mW decrease quickly as the

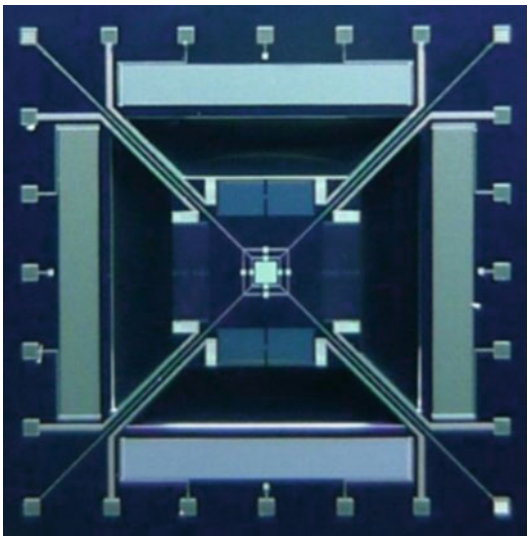

Fig. 11 Micro photograph of the wind sensor presented by Dong et al.

wind velocity increases. As shown in Fig. 23b, the measured values at the wind speed of 2 m/s and 5 m/s are well matched with the fitted curve with error less than 5°.

In 2011, Dong et al. developed a 2D wind sensor operating in TB mode (Dong et al. 2011). As shown in Fig. 24, the sensor is composed of four CTD elements. Each element includes one heater and one temperature sensor. The four CTD elements have been designed and implemented to heat the chip and keep itself at a constant overheat temperature higher than the airflow. Meanwhile, the elements are used to balance the temperature difference between the up-stream and down-stream CTD elements by controlling the heating power of the four heaters. The difference of the heating power between the up-stream and down-stream is a measure for the wind. As shown in Fig. 25, the measured results indicate that the accuracies of the wind sensor are in the range of 0.5 m/s and ±2° at wind speed ranging from 0 to 40 m/s and wind direction from 0° to 360°, respectively.

Sensitivity Improvement and Power Consumption Reduction

In order to obtain high sensitivity and low power consumption, several different methods are always investigated and researched.

Substrate Etching Technology

For the MEMS wind sensor, the heater was fabricated on the silicon substrate before. It is found that most of the produced heat losses in the substrate due to high thermal conductivity of silicon (about 150 W/(m•K)). Therefore, the power consumption is large and the sensitivity is low. From Eq. 2, it can be observed that the temperature

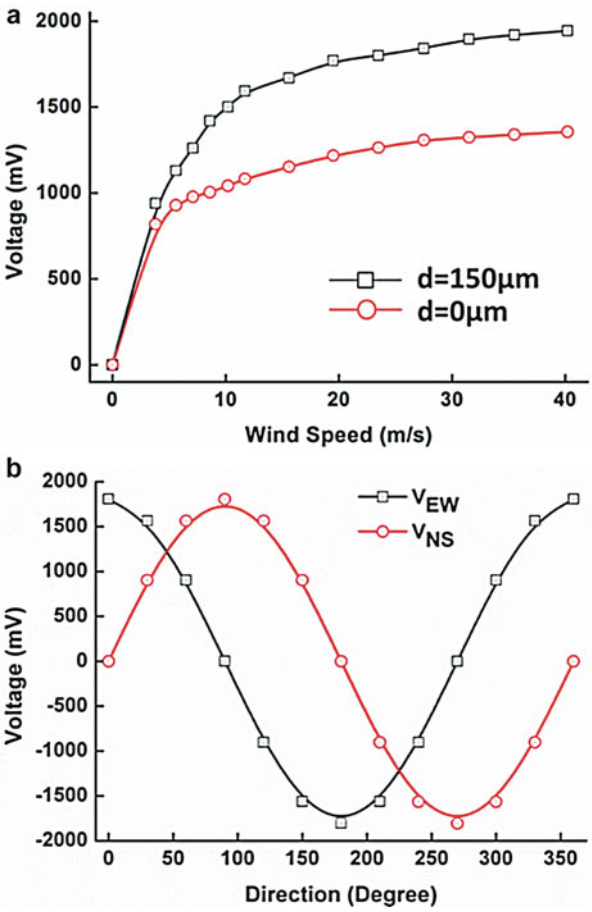

Fig. 12 Tests of the wind sensor presented by Dong et al.: (**a**) wind speed test and (**b**) wind direction test

difference between upstream and downstream is inverse proportional to the substrate thickness. Consequently, for the front surface sensing, the simplest method to solve this problem is to put the wind sensor on the several-micrometer-thickness silicon dioxide or silicon nitride, which is on the surface of the silicon substrate. Then, the substrate is etched to a MEMS membrane and the thermal loss is reduced, as shown in Fig. 26. As a result, most of the heat is interacted with the wind and the sensitivity is improved.

For the back surface sensing, sometimes, trenches are fabricated between the heater and the thermistors, which can reduce the lateral thermal loss, as shown in Fig. 27 (Ye et al. 2017). Figure 28 gives an example of wind sensor with improved sensitivity by trenches technology. The experiments demonstrate that the sensitivity is increased from 9.01 to 16.37 mV/(m/s) at the wind of 3 m/s in CP mode.

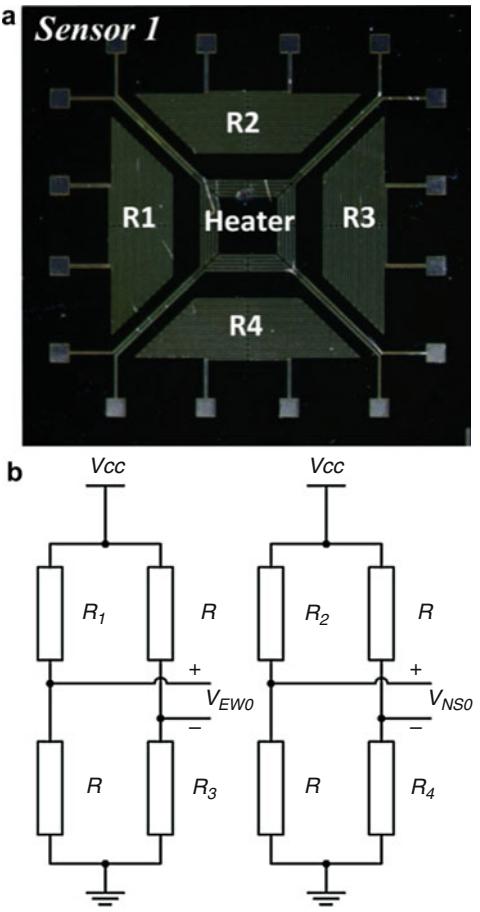

Fig. 13 (**a**) Microphotograph of the thermoresistive wind sensor and (**b**) Wheatstone bridges to measure resistance change

Substrate with Low Thermal Conductivity

In Eq. 2, the smaller the thermal conductivity of the substrate is, the larger the temperature difference is. As a result, in addition to substrate etching technology and trench technology, materials with low thermal conductivity are also chosen as the substrate of wind sensor in order to achieve high sensitivity and low power consumption. Except for silicon dioxide and silicon nitride, ceramic and glass are two common candidates as substrate in micromachined thermal wind sensor. The thermal conductivity is about 20 W/(m•K) and 1.4 W/(m•K) for ceramic and glass, respectively. In 2008, 2D wind thermoresistive sensors are fabricated on ceramic and glass substrate (Shen 2009), respectively. As shown in Fig. 29, Pt is lifted off to form the heating and sensing elements. The measured results are recorded in Fig. 30. It is seen that the power consumption is less than 50 mW and the measurement range is

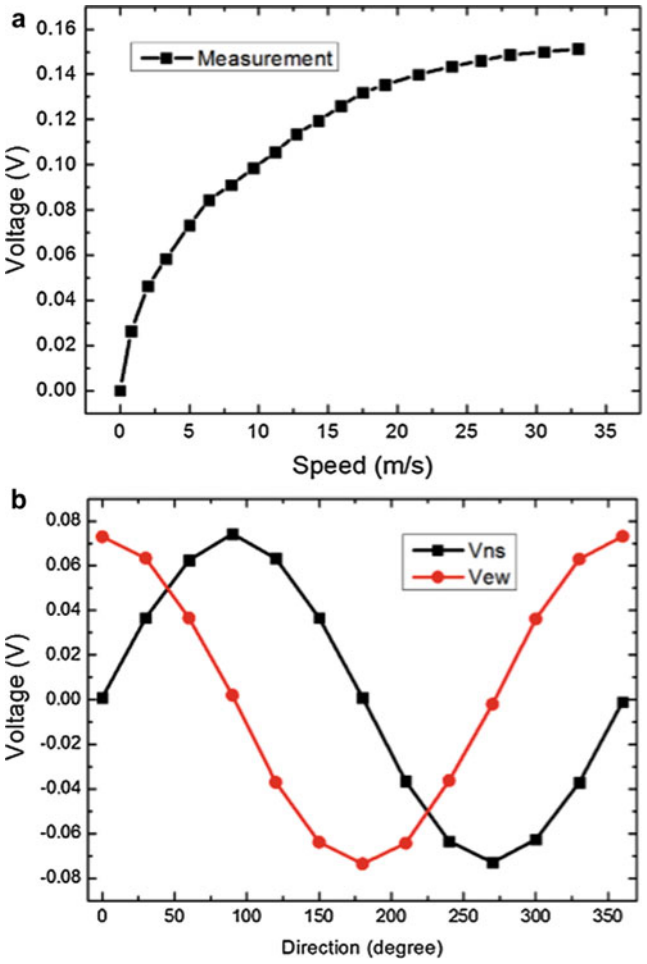

Fig. 14 Measured results of the thermoresistive wind sensor: (**a**) wind speed and (**b**) wind direction

from 0 to 10 m/s. Above all, the sensitivity is improved by ten times compared with the traditional silicon wind sensor. However, the flatness in the surface of ceramic substrate limits its application.

In Fig. 31, in 2014, Gu et al. fabricated a thermoelectric wind sensor on ceramic substrate for the first time (Gu 2012; Zhu et al. 2014). Nickel heaters and four Ni/Al thermopiles are directly fabricated on the front surface of the ceramic plate while the back side is exposed to the wind as the sensing surface. The whole process is simple and the sensor substrate is used directly as a packaging board for sensing wind. The sensor is tested in CP mode. Experimental results in Fig. 32 show that this wind sensor can measure wind speeds up to 30 m/s and wind direction in a full range of 360°.

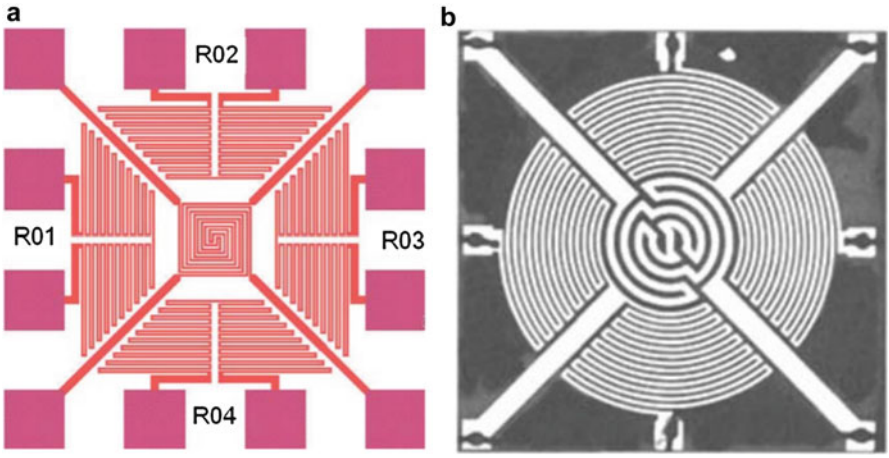

Fig. 15 (**a**) Layout of the thermoresistive wind sensor with square structure and (**b**) micrograph of the wind sensor with circular structure

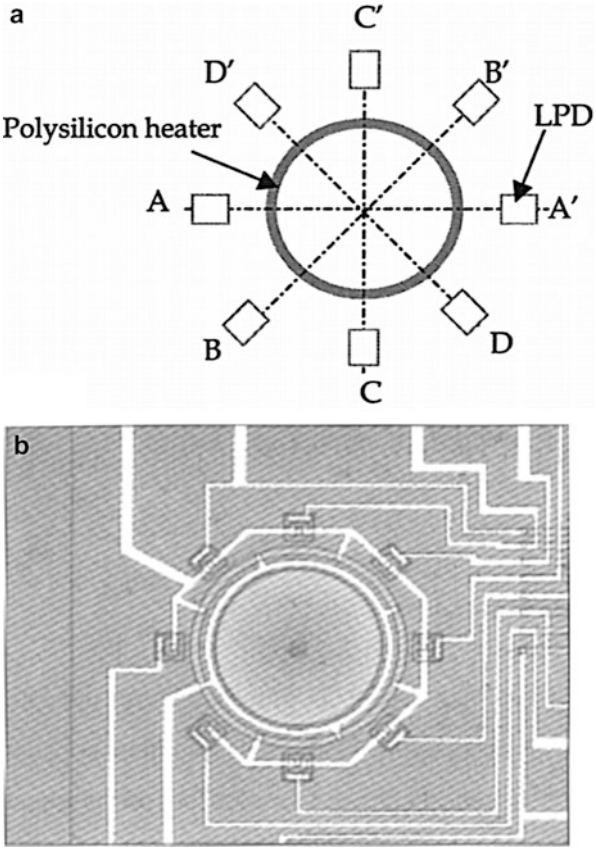

Fig. 16 Thermoelectronic wind sensor proposed by Qin: (**a**) schematic overview and (**b**) micro photograph

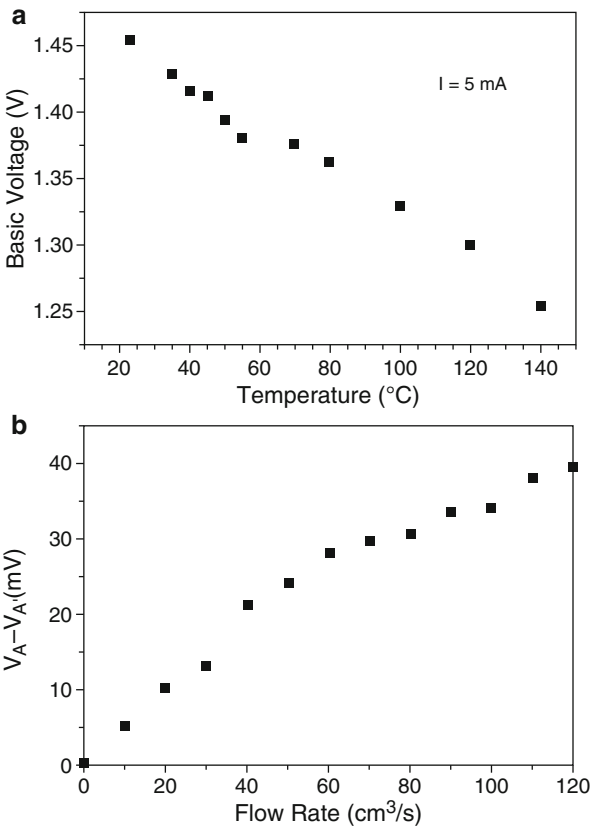

Fig. 17 Measured results of the thermoelectronic wind sensor: (**a**) bias voltage change with temperature and (**b**) voltage difference between LCP A and LCP A′

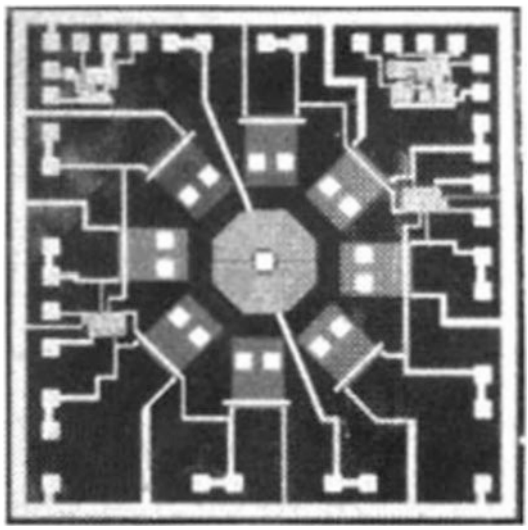

Fig. 18 Micrograph of the thermoelectronic wind sensor by Wu et al.

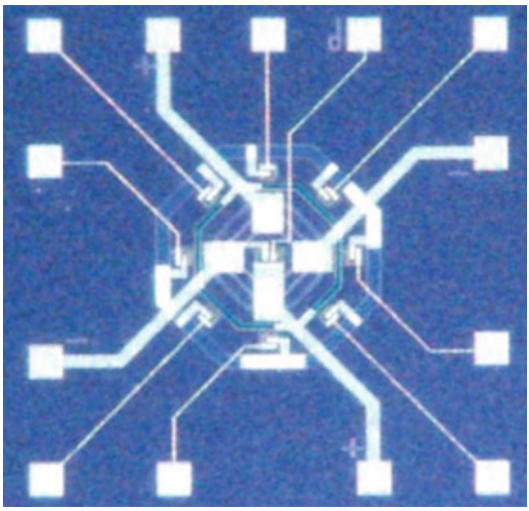

Fig. 19 Micro photograph of the thermoelectronic wind sensor by Sun et al.

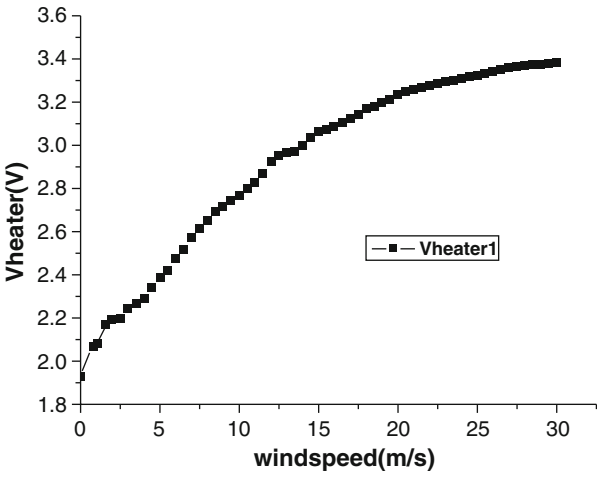

Fig. 20 Measured heating voltage changing with wind speed up to 30 m/s

Full-Bridge Technology

As shown in Fig. 33, in the traditional wind sensor, four thermistors are fabricated to a square around the heater symmetrically (Shen et al. 2008). The thermistor R1 and R3 both act as one of four resistors in a Wheatstone bridge and the voltage is proportional to wind speed. Figure 33b shows this structure named half-bridge structure. Shen et al. designed two thermistors located at different distances from

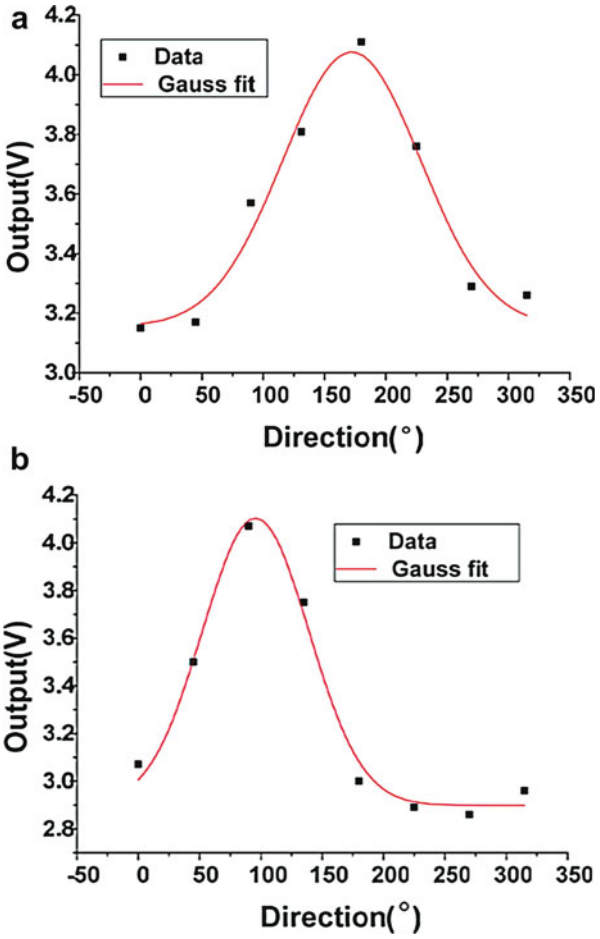

Fig. 21 Wind direction fitting by Gauss function: (**a**) the direction is 180° and (**b**) the direction is 90°

the central heater in each direction, as shown in Fig. 34a. Therefore, four thermistors including R11, R12, R31, and R32 constitute a Wheatstone full bridge. When the wind blows, R31 and R32 increase while R11 and R12 decrease. By the connection way in Fig. 34b, the output voltage can be increased and the sensitivity is improved. Moreover, the measurement range of the wind sensor is also expanded because two thermistors are connected in series in different location to the heater. Figure 35 shows the micro photograph of the wind sensor with full bridge technology. The measured results of wind speed and direction are recorded in Fig. 36a, b, respectively. The measurements demonstrate that the sensitivity is close to 10 mV/(m/s) and the range is up to 35 m/s based on calorimetric principle.

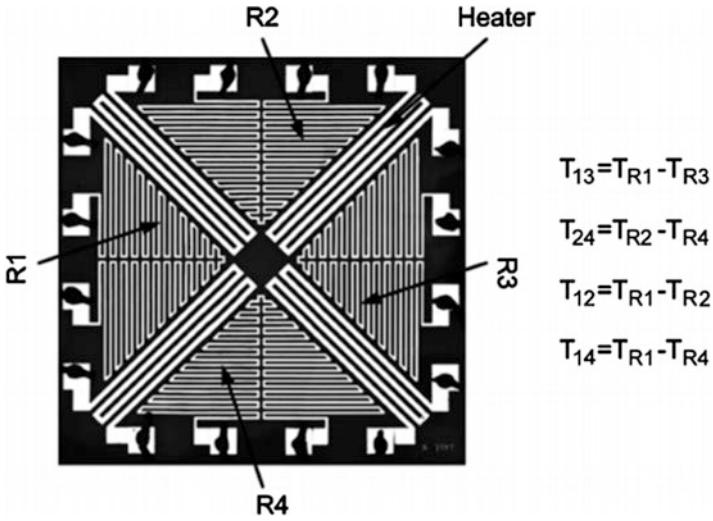

Fig. 22 Micro photograph of the wind sensor to realize self-test function by Shen et al.

Other Methods

Except the methods above, Zhu et al. proposed a novel wind sensor with improved sensitivity and low consumption using back surface sensing (Zhu et al. 2015), as shown in Fig. 37. The silicon with holes is anodic bonded to the glass and reflow is performed with high temperature. Thus, the holes are filled with glass and the silicon is thinned until the glass appears. Heating and sensing resistors are fabricated on the silicon substrate. As a result, the heat conduction is suppressed and the heat convection is enhanced. Figure 38 gives the microphotograph of front surface and back surface of the fabricated sensor. The experimental results are recorded and the power consumption can be reduced to less than 20 mW. As shown in Fig. 39, this wind sensor can measure the speed from 0 to 30 m/s and the direction from 0° to 360°.

On this basis, the power consumption is further reduced by using HF wet etching (Zhu et al. 2016). After wet etching, the thickness of the glass substrate decreases, so that the sensor's thermal vias become more exposed to the wind, as shown in Fig. 40a. As a result, the conductive heat transfer is weakened and the convective heat transfer is enhanced in sensor operation. Before and after wet etching for 7 and 14 min in Fig. 40b, at the wind speed of 5 m/s, the measured sensitivities of the sensor with a total power consumption of 24.5 mW are 77.2, 98.6, and 164.1 mK/(m/s).

In addition to the methods above, for the thermoelectric wind sensor based on Seebeck effect, the two materials with large difference of Seebeck coefficient will also increase the output voltage. For example, P+ polysilicon reveals positive

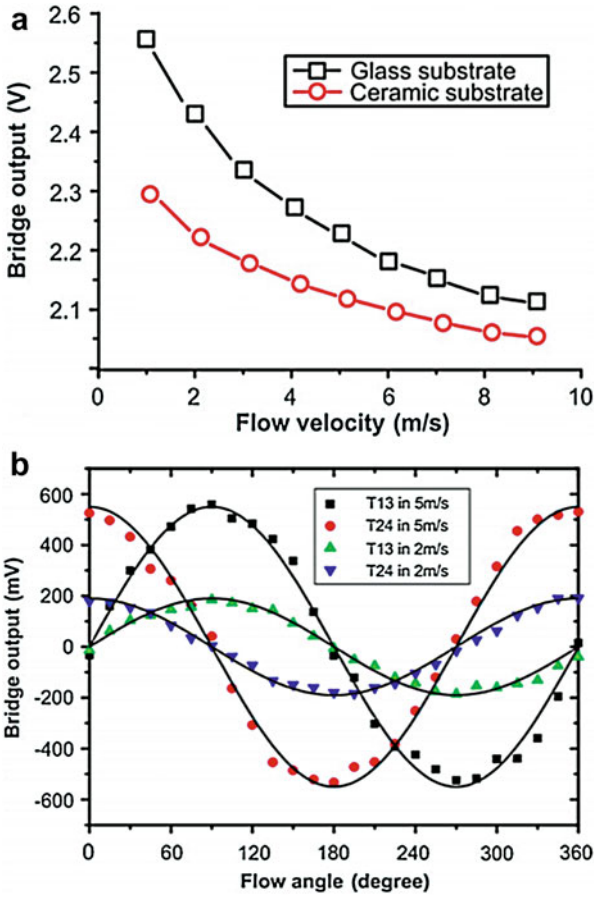

Fig. 23 Experiments of the wind sensor with self-test function: (**a**) wind speed experiment and (**b**) wind direction experiment

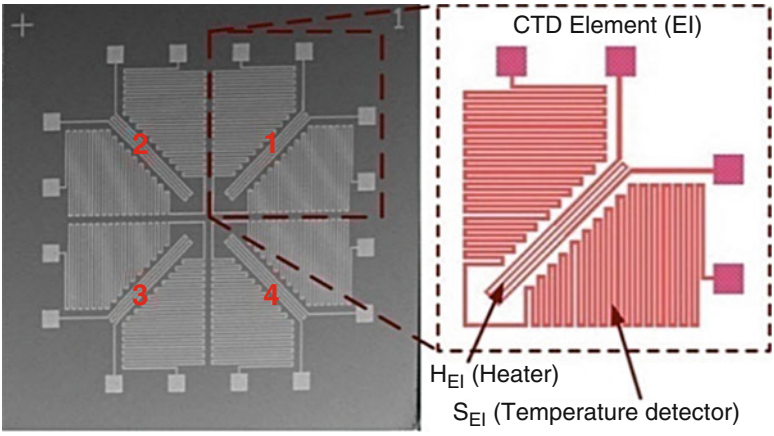

Fig. 24 Micro photograph of the wind sensor working in TB mode

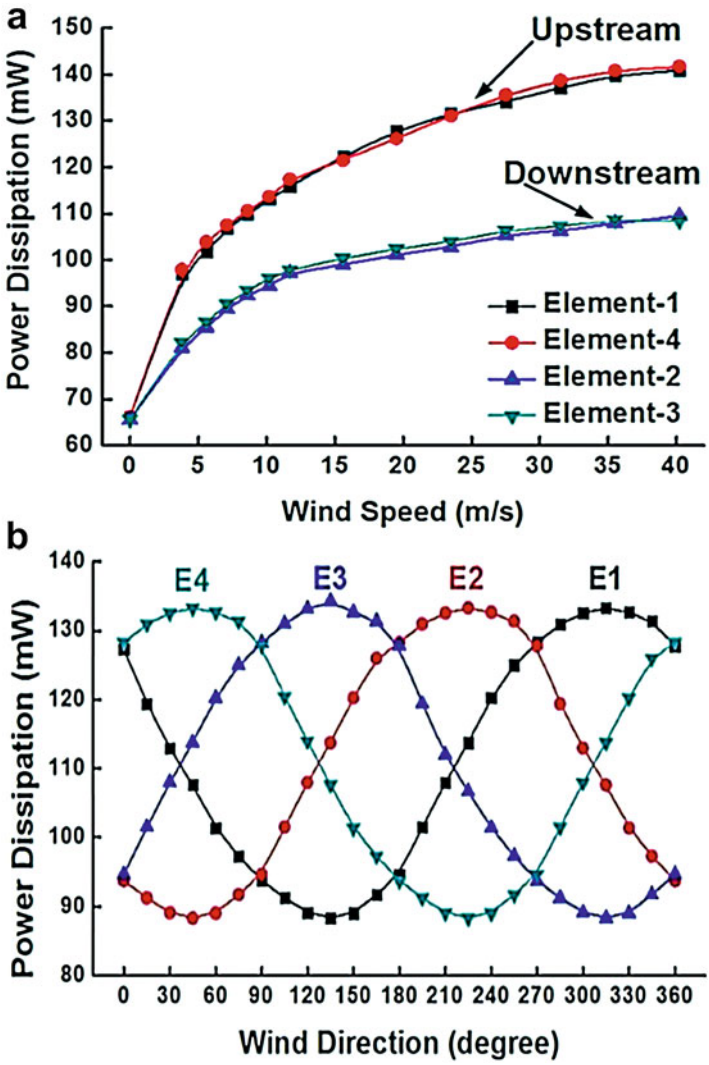

Fig. 25 (**a**) Wind speed measurement and (**b**) direction measurement of the wind senor in TB mode

Seebeck coefficient while N+ polysilicon has negative Seebeck coefficient. These two materials are combined and a large voltage can be obtained. However, this will increase the difficulty in fabrication. For the thermoresistive wind senor, the thermistors with high temperature coefficient of resistance, such as Ge, can help to increase the output signal and improve the sensitivity of the sensor. Moreover, square wave signal with a certain duty cycle instead of DC signal can be applied to the heater and low power consumption is achieved.

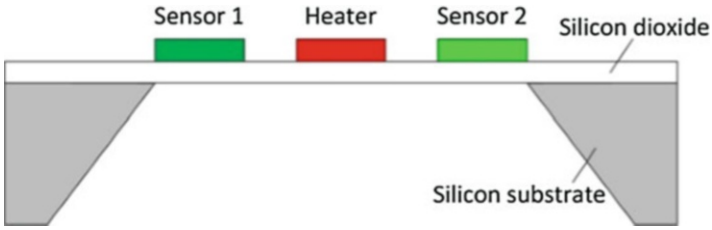

Fig. 26 Schematic of the wind sensor fabricated on a MEMS membrane by substrate etching technology

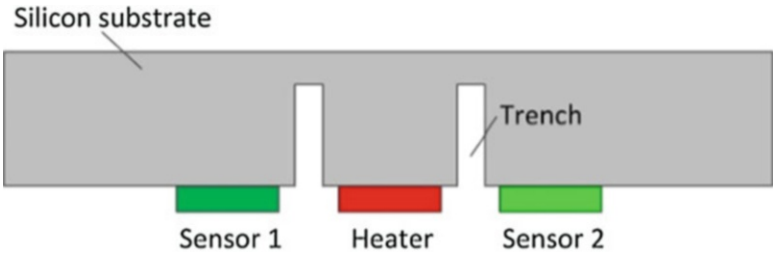

Fig. 27 Schematic of the wind sensor with trenches between the heater and the thermistors

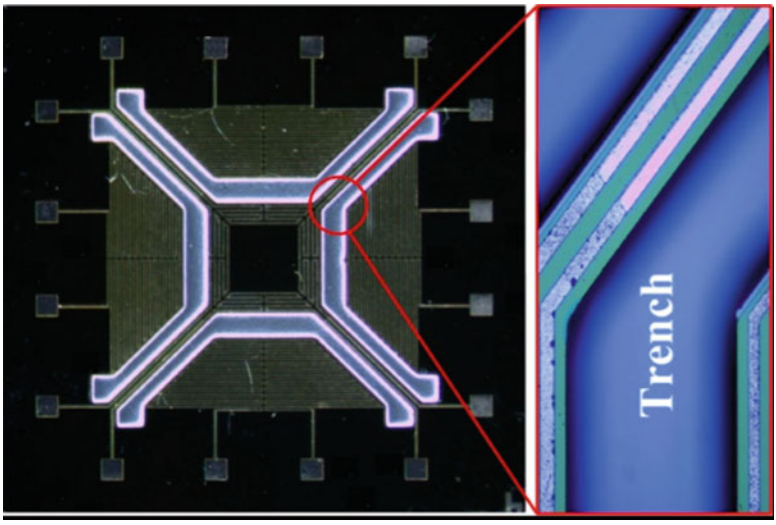

Fig. 28 Micro photograph of the wind sensor with trenches between the heater and the thermistors

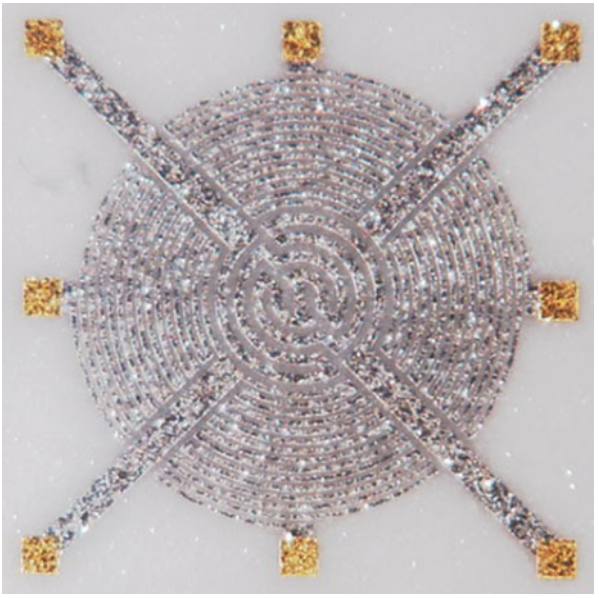

Fig. 29 Micrograph of the wind sensor fabricated on ceramic substrate

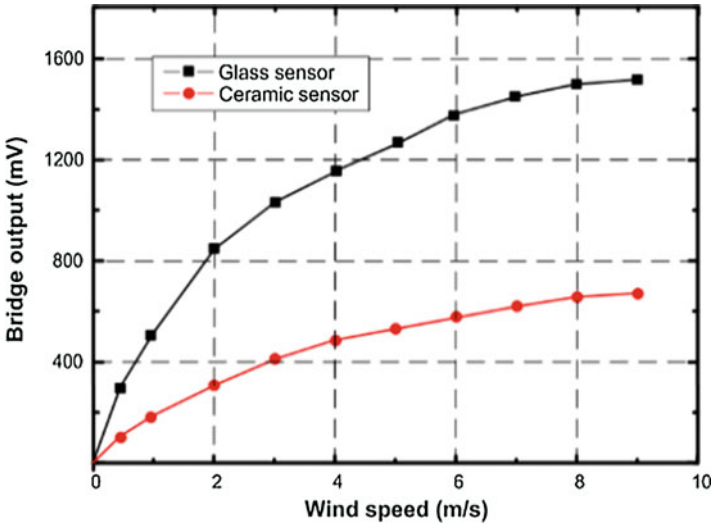

Fig. 30 Speed measurement of the thermoresistive wind sensor fabricated on ceramic and glass substrate

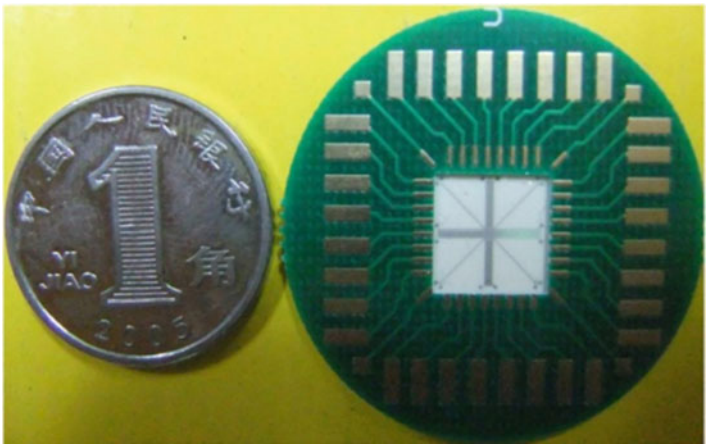

Fig. 31 Micrograph of the thermoelectric wind sensor fabricated on ceramic substrate

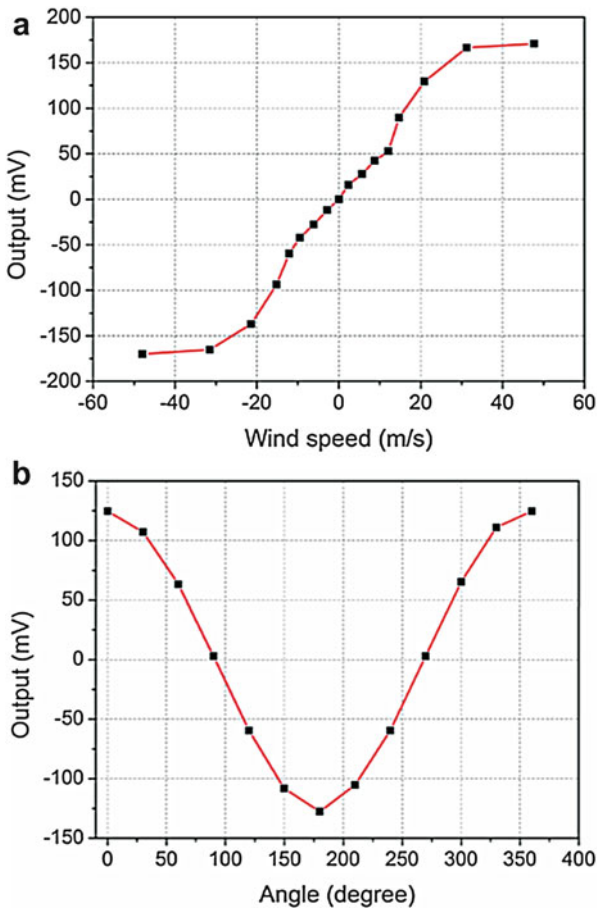

Fig. 32 Experiments of the thermoelectric wind sensor fabricated on ceramic substrate: (**a**) wind speed experiment and (**b**) wind direction experiment

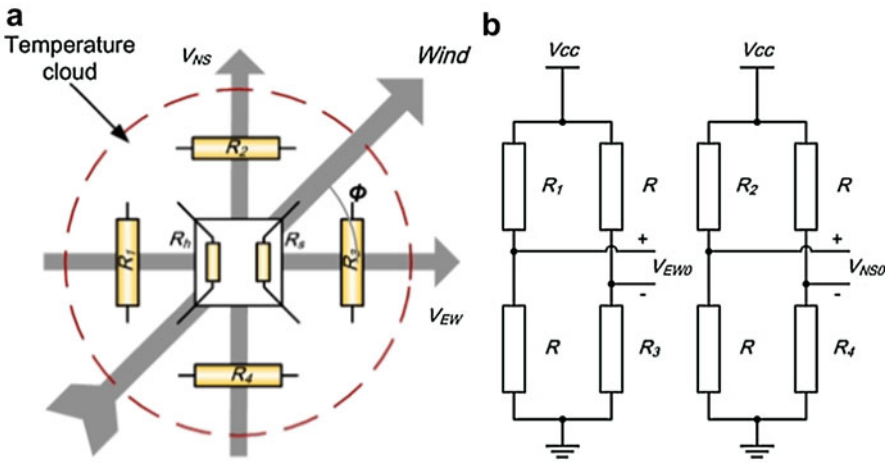

Fig. 33 (**a**) Schematic diagram of the wind sensor and (**b**) circuits with half bridge technology

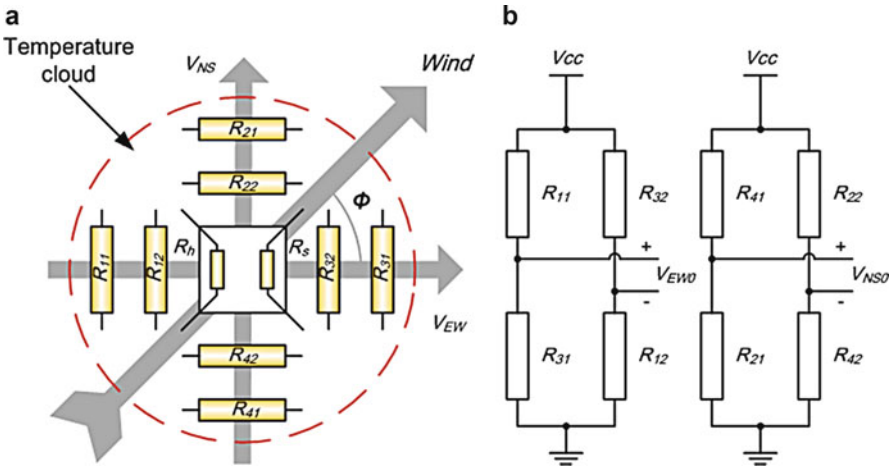

Fig. 34 (**a**) Schematic diagram of the wind sensor and (**b**) circuits with full bridge technology

Package

Different from other flow sensors, the wind sensor is placed outside and is easy to be polluted by particles and rain in the air. Therefore, package is necessary and three different package methods are widely used in MEMS thermal wind sensor.

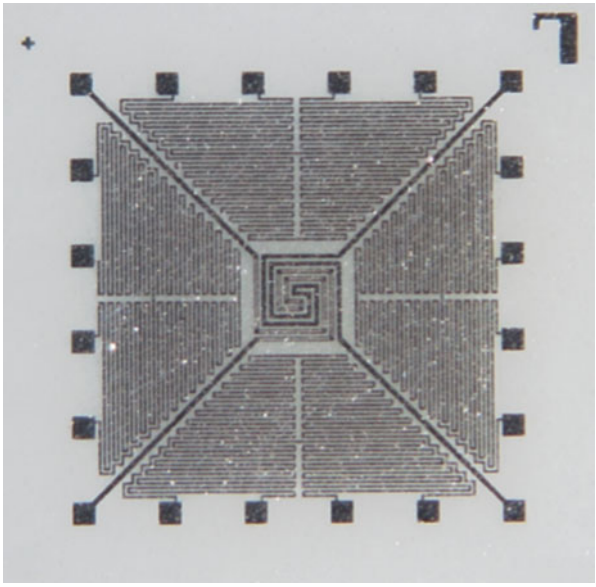

Fig. 35 Micro photograph of the wind sensor with full bridge technology on ceramic substrate

Direct Chip Attach Package

The simplest method is direct chip attach (DCA) package. As shown in Fig. 41a, the front surface of the chip is glued to one side of a FR4 substrate while the back surface is used to sense wind change (Shen et al. 2008). The contacting pads in the chip are bonded by wires and connected to processing circuits in the FR4 substrate. Finally, encapsulant such as epoxy resin is used to protect the sensor and the bonding wires. Figure 41b shows the schematic and microphotograph of the wind sensor by DCA package, respectively.

Flip Chip Package

The second package is flip chip (FC) package. As shown in Fig. 42a, Au and Pb/Sn bumps are fabricated on chip and FR4 substrate (Sun et al. 2010), respectively. Then, these two kinds of bumps are welded using a vacuum chuck at about 240 °C. In order to enhance the mechanical strength, epoxy-based underfill is applied. Figure 42b gives the wind sensor with Au bumps and FR4 substrate with Pb/Sn bumps.

Additionally, Sun et al. proposed a FC package to ceramic substrate (Sun et al. 2005, 2007), as shown in Fig. 43a. The sensor chip was fabricated by standard CMOS technology, and it is FC packaged on a thin ceramic substrate using copper pillar bump technology. In Fig. 43b, heat transfer is performed between the heaters

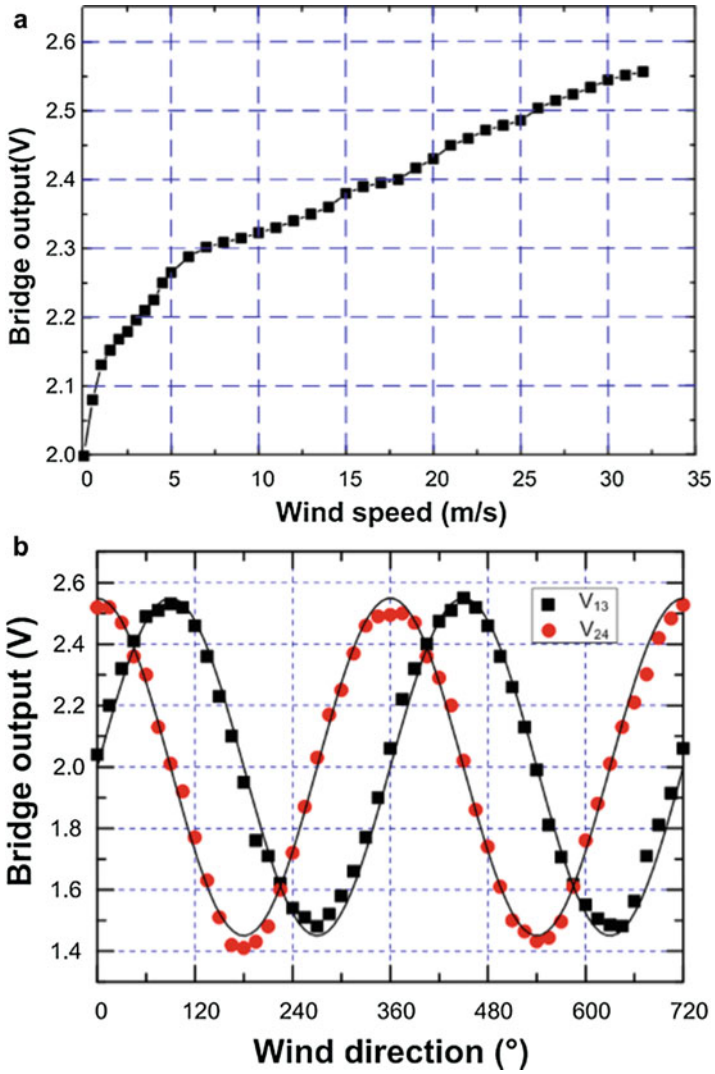

Fig. 36 Measurement of the wind sensor with full bridge technology: (**a**) speed measurement and (**b**) direction measurement

and the ceramic substrate via the pillar bump. The backside of the ceramic substrate provides a smooth surface for the sensor to contact with the flow. The change of flow-induced temperature distribution on the flow sensing surface is measured by temperature sensors. Meanwhile, the ceramic substrate holds the sensor chip and protects it from being contaminated or even destroyed in harsh environment.

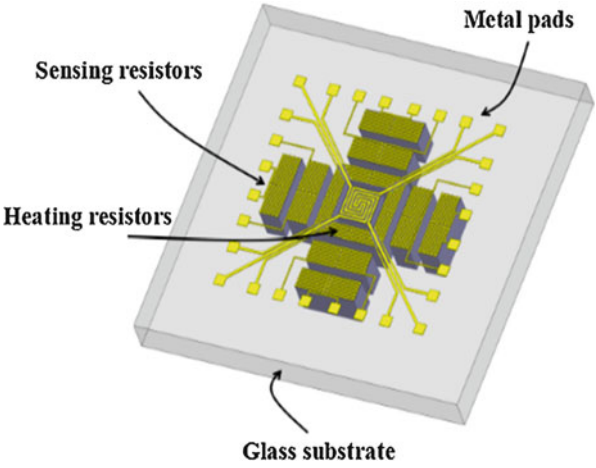

Fig. 37 Schematic diagram of the wind sensor by Zhu et al.

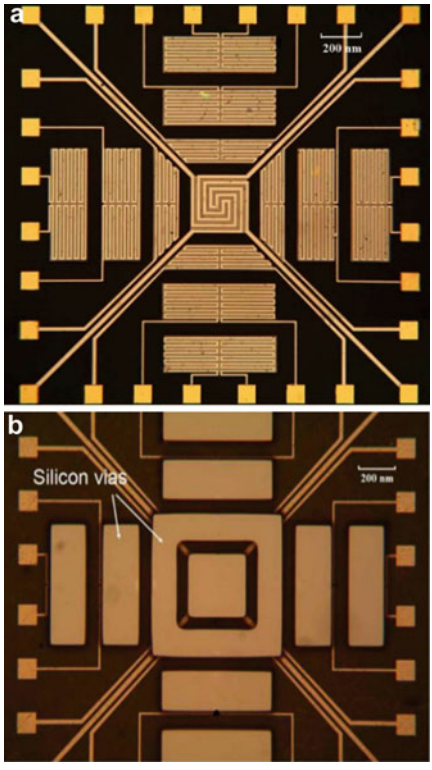

Fig. 38 Microphotograph of the wind sensor by Zhu: (**a**) front surface and (**b**) back surface

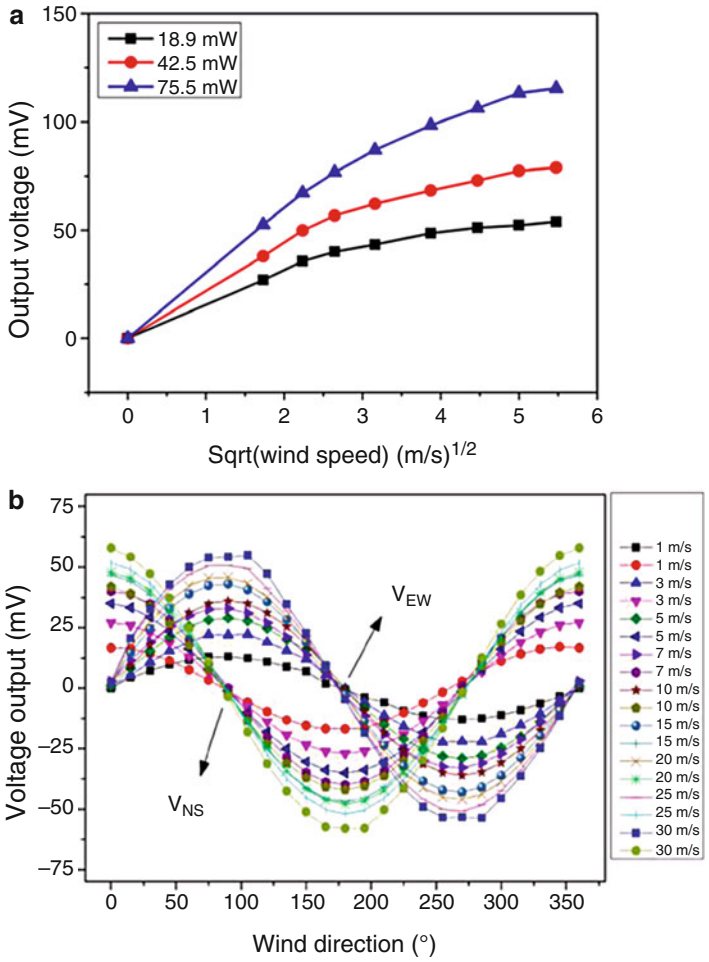

Fig. 39 Measured results of the wind sensor by Zhu: (**a**) wind speed and (**b**) wind direction

Au-Au Bonding Package

In 2012, Dong et al. proposed a novel package method by Au-Au wafer bonding technology (Dong et al. 2011, 2012). As shown in Fig. 44a, the sensing parts are fabricated on the silicon substrate using standard IC process, while the heating parts are designed on the ceramic substrate. Au bumps are fabricated on these two substrates and the thickness is about 5 μm. The Au-Au bonding is performed at 380 °C

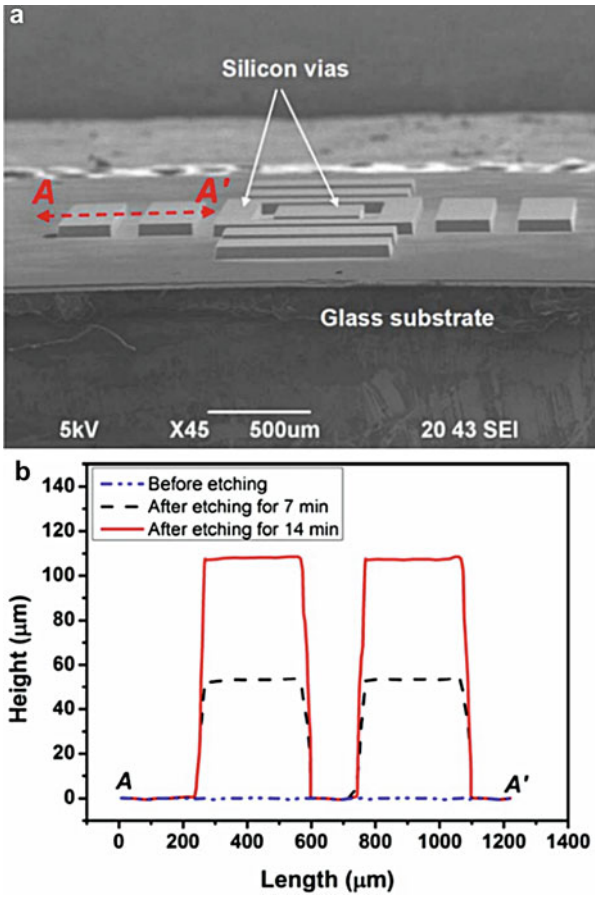

Fig. 40 (**a**) The SEM photograph of the wind sensor after wet etching. (**b**) Step height lines of the sensor surface in different etching time by step profiler

for about 30 min. One kind of the Au bumps is used for electric connection between silicon substrate and ceramic substrate while the other kind is used for thermal connection between two substrates. After that, the redundant silicon is removed by the wet etching, as shown in Fig. 44b. Figure 45 presents the microphotograph of the wind sensor before and after Au-Au bonding package.

Environmental Effect

The wind sensor is placed outside and easily affected by the environment although the package is performed. Obviously, ambient temperature has an effect on the wind sensor due to its thermal principle.

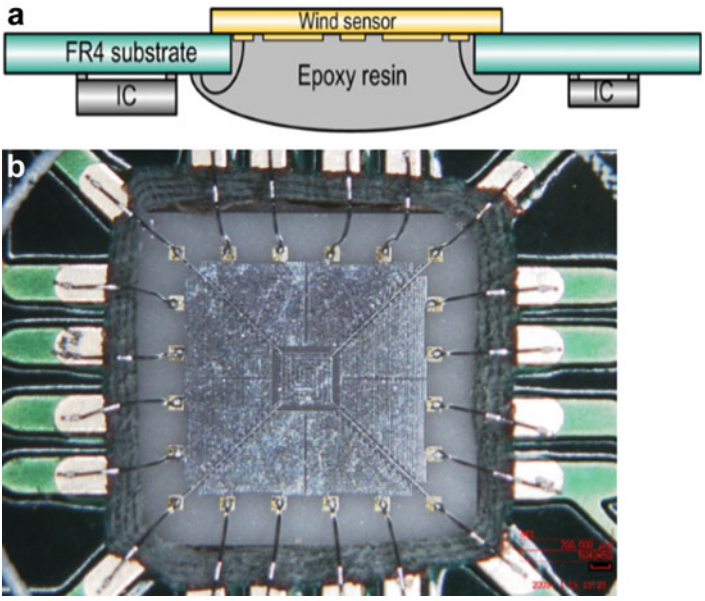

Fig. 41 (**a**) Schematic of the DCA package and (**b**) microphotograph of the wind sensor after DCA package

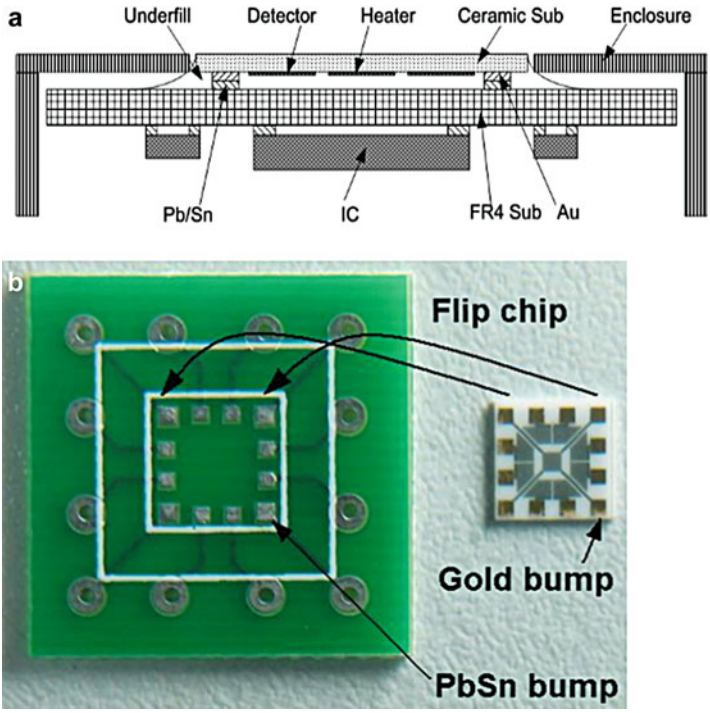

Fig. 42 (**a**) Schematic overview of the FC package and (**b**) photo of the wind sensor and FR4 substrate by FC package

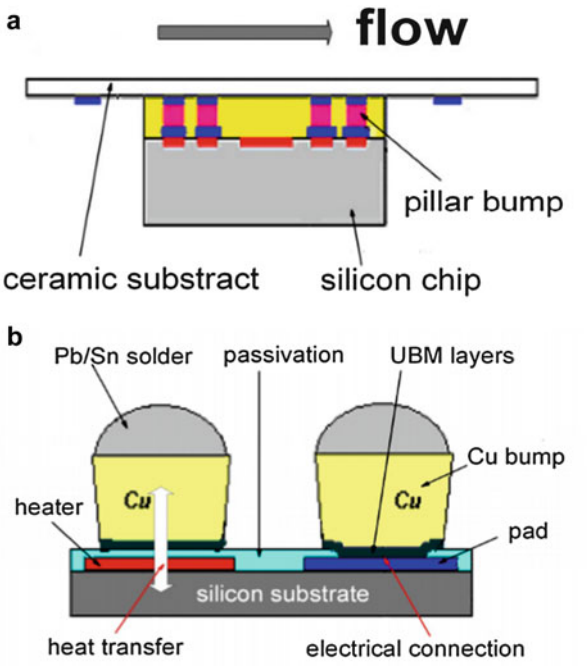

Fig. 43 (**a**) Schematic overview of the FC package to ceramic and (**b**) copper pillar bump structure

Temperature Effect

Huang et al. researched the temperature effect on the micromachined thermal wind sensor (Huang et al. 2015; Chen et al. 2015). Figure 46 displays the measured output voltage change in 10 m/s when the ambient temperature increases from −20 °C to 40 °C. A linear curve is fitted and the slope is close to 1.25 mV/k. In addition, a theoretical model is established and temperature compensation is performed. Figure 47 shows the wind speed measurement result with temperature compensation using the proposed model. As can be observed, after compensation, the relative error of the wind speed measurement at different ambient temperatures is less than ±3.5%.

Humidity Effect

Humidity effect is also investigated by Chen et al. in 2014 (Chen et al. 2014). The experimental results are obtained by testing the sensor in sunny day and rainy day. Figure 48 shows the output voltage for the relative humidity of 52% and 70% at 23 °C. The experimental results indicate that the output voltage decreases with the

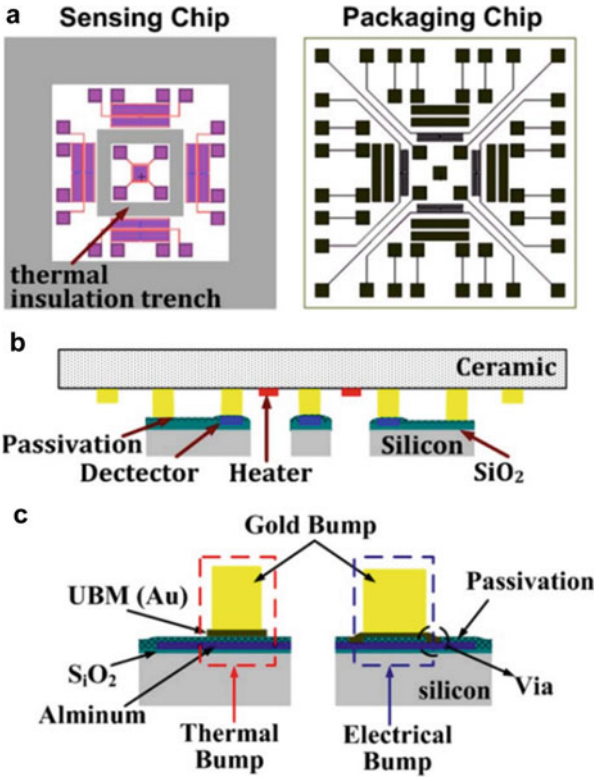

Fig. 44 (**a**) Schematic overview of layout of two chips, (**b**) cross-section of the Au-Au bonding technology and (**c**) gold bumps for thermal exchange and electrical connection

increase of the humidity. The effect of relative humidity on the output is less than 1%, which is not obvious compared with the temperature effect.

Conclusion

Micromachined thermal wind sensor is introduced in this chapter. Different principles and operation modes are addressed. Several typical wind sensors including 1D and 2D devices are given and the related measurements are also presented. The wind speed measuring dynamic range exceeds 0–40 m/s with the direction from 0° to 360°. Several methods are considered and analyzed, and the power consumption can be reduced to less than 20 mW. In application, the MEMS wind sensor can be packaged using various packages such as DCA package, FC package, and Au-Au bonding package. Despite this, the wind sensor is easy to be affected by the surrounding temperature. Related measurements are given and the temperature effect is modeled.

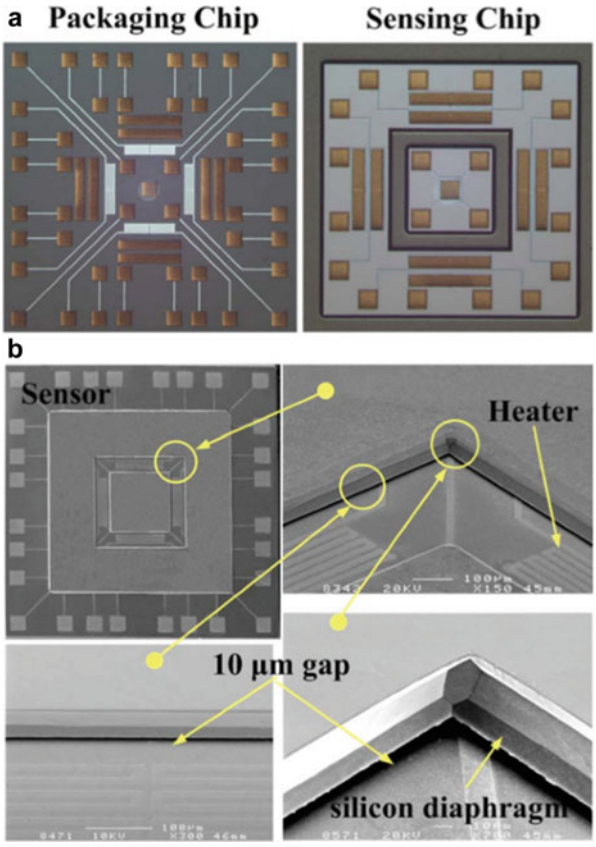

Fig. 45 Microphotograph of the wind sensor of (**a**) before and (**b**) after Au-Au bonding package

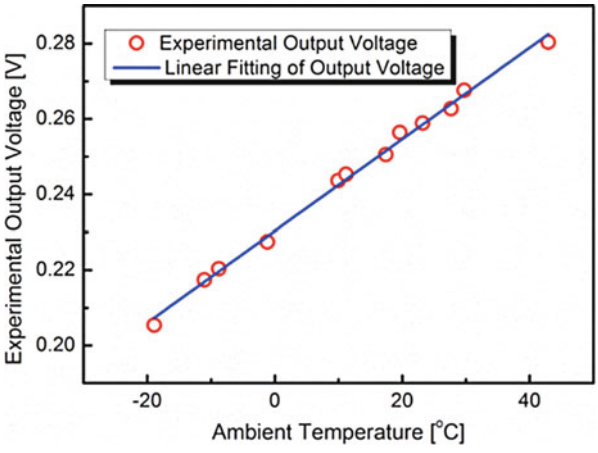

Fig. 46 Measurement of temperature effect on MEMS wind sensor in the wind speed of 10 m/s

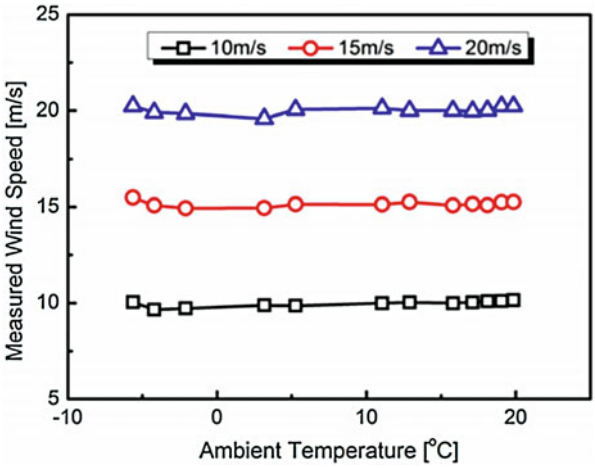

Fig. 47 Measured wind speed of the sensor in different ambient temperatures with temperature compensation

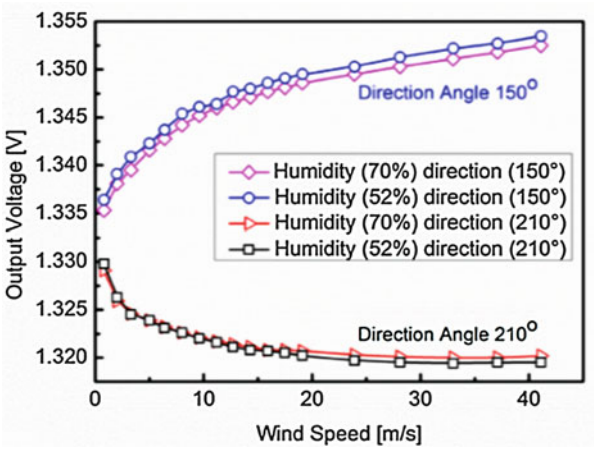

Fig. 48 Measurement of humidity effect on the MEMS wind sensor

References

Chen B, Zhu Y, Qin M et al (2014) Effects of ambient humidity on a micromachined silicon thermal wind sensor. J Microelectromech Syst 23(2):253–255

Chen B, Zhu Y, Yi Z et al (2015) Temperature effects on the wind direction measurement of 2D solid thermal wind sensors. Sensors 15(12):29871–29881

Cheng H, Qin M, Gao D (2004) Thermal-film temperature-difference-based CMOS wind sensor design and realization. Chin J Electron Devices 27(3):486–489

Dong Z (2012) Study on MEMS wind sensors and control system. PhD dissertation, Southeast University

Dong Z, Chen J, Qin Y et al (2011) A hot film wind sensor with four constant temperature difference elements fabricated on ceramic substrate. In: Proceeding of IEEE sensors. Limerick. 28–31 Oct 2011

Dong Z, Chen J, Qin Y et al (2012) Fabrication of a micromachined two-dimensional wind sensor by Au-Au wafer bonding technology. J Microelectromech Syst 21(2):467–475

Durst F, Al-Salaymeh A, Bradshaw P (2003) The development of a pulsed-wire probe for measuring flow velocity with a wide bandwidth. Int J Heat Fluid Flow 24:1–13
Gao D, Qin M, Cheng H (2004) Optimization and test of a calorimetric silicon flow sensor. In: International conference on information acquisition, Hefei. 21–25 June 2004
Giani A, Mailly F, Bonnot R (2002) Thermal model of thin film anemometer. Microelectron J 33(8):619–625
Gu F (2012) A study to the thermopile ceramic wind sensor. Master's thesis, Southeast University
Huang Q, Chen B, Zhu Y et al (2015) Modeling of temperature effects on micromachined silicon thermal wind sensors. J Microelectromech Syst 24(6):2033–2039
Huijsing JH, Schuddemat JP, Verhoef W (1984) Monolithic integrated direction-sensitive flow sensor. IEEE Trans Electron Devices 29(1):57–60
Kato N, Ohkuma T, Kim JR (1992) Full scale measurements of wind velocity in two urban areas using an ultrasonic anemometer. J Wind Eng Ind Aerodyn 41(1):67–78
King LV (1914) On the convection of heat from small cylinders in a stream of fluid. Philos Trans R Soc Lond Ser A 214:373–432
Kuo JTK, Yu L, Meng E (2012) Micromachined thermal flow sensors-a review. Micromachines 3:550–573
Makinwa KKA (2004) Flow sensing with thermal sigma-delta modulators. PhD dissertation, Delft University of Technology
Oudheusden BWV (1988) Silicon flow sensors. Control Theory Appl IEE Proc DIET 135(5):373–380
Oudheusden BWV (1990) Silicon thermal flow sensor with a two-dimensional direction sensitivity. Meas Sci Technol 1(7):565–575
Qin M, Huang Q, Zhang Z et al (2001) A novel micromachined thermal anemometer based on laterally polysilicon diode flow sensor. In: Proceedings of the SPIE 4601, micromachining and microfabrication process technology and devices, 15 Oct 2001
Shen G (2009) System integration and packaging of thermal wind sensor. PhD dissertation, Southeast University
Shen G, Wu J, Zhang H et al (2007) Design and test of 2-D MEMS wind speed and direction sensor. Micronanoelectron Technol 7(8):285–287
Shen G, Qin M, Huang Q (2008) A zmart 2-D wind sensor with self-test function. In: Proceeding of IEEE sensors 2008, Lecce. 26–29 Oct 2008
Shen G, Qin M, Huang Q (2010) A cross-type thermal wind sensor with self-testing function. IEEE Sensors J 10(2):340–346
Sun J (2006) Design and package of CMOS thermal flow sensors. Master's thesis, Southeast University
Sun J, Qin M, Huang Q (2005) A flip-chip packaged CMOS thermal flow sensor. In: Proceeding of IEEE sensors, Irvine. 30 Oct–3 Nov 2005
Sun J, Qin M, Huang Q (2007) A flip-chip packaged CMOS thermal flow sensor. IEEE Sensors J 7(7):990–995
Wu J, Qin M (2006) Study on integrated controlling and measuring circuits of the two-dimensional CMOS silicon wind sensor. Chin J Electron Devices 29(1):95–101
Wu J, Sansen W (2002) Electrochemical time of flight flow sensor. Sensors Actuators A Phys 97:68–74
Ye Y, Yi Z, Qin M et al (2017) DRIE trenches and full-bridges design for sensitivity improvement of MEMS silicon thermal wind sensor. In: Proceeding of 30th IEEE international conference on micro electro mechanical systems, Las Vegas, 22–26 Jan 2017
Zhang Z, Qin M, Huang Q (2002) Novel CMOS two-dimensional integrated gas flow sensor. In: Proceedings of SPIE, micromachining and microfabrication process technology and devices, Oct 2001
Zhu Y, Chen B, Qin M et al (2014) 2D micromachined thermal wind sensors-a review. IEEE Internet Things J 1(3):216–230
Zhu Y, Chen B, Qin M et al (2015) Development of a self-packaged 2D MEMS thermal wind sensor for low power applications. J Micromech Microeng 25:055011
Zhu Y, Qin M, Huang J et al (2016) Sensitivity improvement of a 2D MEMS thermal wind sensor for low-power applications. IEEE Sensors J 16(10):4300–4308